J Therm Anal Calorim (2011) 104:577–583
DOI 10.1007/s10973-010-0988-1

Low-temperature synthesis and characterization of the Mn–Zn ferrite

Irena Szczygiel · Katarzyna Winiarska

Received: 14 June 2010 / Accepted: 28 July 2010 / Published online: 18 August 2010

Abstract Nanocrystalline ferrite with the composition: $Mn_{0.6}Zn_{0.4}Fe_2O_4$ was synthesized by two-stage route: the precipitation of Zn, Mn and Fe hydroxides from sulphates solution and the synthesis of a precursor by the sol–gel auto-combustion method. The ferrite powder obtained from the gel by ashing was sintered under air at a temperature of 720, 1150 and 1300 °C. The composition and morphology of the as-obtained phases were examined by ICP-AES, TG/DTA, XRD, FTIR, SEM and low-temperature nitrogen adsorption (BET). It was found that the spinel phase forms after gel combustion. The nanometric ferrite powder obtained as a result of the combustion is soft-agglomerated. The zinc content in the ferrite during ashing and auto-combustion is lower by about 21 mol% than the assumed one and the final product turn out to be $Mn_{0.68}Zn_{0.32}Fe_2O_4$.

Keywords Mn–Zn ferrite · Nanomaterials · Co-precipiation · Sol–gel preparation

Introduction

As soft magnetic materials Mn–Zn ferrites are commonly used in microelectronics, e.g. in transformer cores, choke coils and electromagnetic interference devices (EMI). They owe their wide application range to their properties such as: high initial magnetic permeability, electrical resistivity and low core losses at high frequencies. On the industrial scale, ferrites are produced from proper metal oxides or carbonates, using the ceramic method. However, this method involves many stages and it is energy-consuming [1–3].

In recent years research into the synthesis of Mn–Zn ferrites by chemical methods: sol–gel and sol–gel auto-combustion [4–9], hydrothermal [10, 11], co-precipitation [12] and reversed micelles [13] have been conducted. The material produced by chemical methods is homogenous and with uniform particle size distribution, and the low synthesis temperature favours the formation of particles from a few to over 10 nm in size. The change in particle size from micrometres to nanometric size affects the properties of the ferrite material. When particle size is below 20 nm, nanocrystalline ferrites are characterized by superparamagnetism, the material becomes monodomain, and thermal energy causes fluctuations in the particle magnetization vector [14]. Materials produced by chemical methods have new unique properties whereby they can be applied in new fields of science and technology, for example, in biomedicine and as catalysts or gas sensors [14–18].

One of the most attractive methods of producing oxide materials, including ferrites, is the sol–gel auto-combustion method. It is based on a proper selection of oxidation and reduction reactions between the fuel and the oxidizer during which heat is rapidly released and locally the temperature of the reagents momentarily rises to as high as 3000 °C. The choice of an organic compound as the fuel for the combustion reaction and its molar ratio to the oxidizer significantly affects the quality of the obtained product. Citric acid, urea and glycine (formerly also hydrazine and its compounds) are most often used as the fuel. Nitrate (V) ions, introduced as metal nitrates or nitric acid into the solution, perform the function of the oxidizer. In the combustion process, the nitrates are decomposed to

I. Szczygiel (✉) · K. Winiarska
Department of Inorganic Chemistry, Faculty of Engineering and Economics, Wroclaw University of Economics, Wroclaw, Poland
e-mail: irena.szczygiel@ue.wroc.pl

nitrogen (II, IV and V) oxides. The fuel complexes the metal ions in the solution whereby a homogenous mixture is obtained. It is also a source of hydrogen and carbon, which as a result of combustion forms H_2O and CO_2 and supply heat. The auto-combustion reaction is exothermic, and the temperature reaches 1000–3000 °C. The high temperature is conducive to the formation of high purity powders. The rate of combustion and the large volume of the liberated gases inhibit the growth and crystallization of particles and thereby favour the formation nanometric size particles with high specific surface area [19, 20].

In this paper, we showed unique combination of two well-known method of synthesis ferrite which was used to obtained nanocrystalline ferrite. A precursor to sol–gel auto-combustion method was synthesized by co-precipitation. Mn–Zn ferrite could be obtained from this precursor in high-temperature sintering but the product is coarsed, whilst application of sol–gel auto-combustion method allows to produce nanocrystalline ferrite in low temperature (ca 400 °C). Unfortunately, this method could not be used to synthesize ferrite powder from sulphate solutions because the sulphates constituted secondary phase in obtained material after combustion process. Thus, in this research, nanometric Mn–Zn ferrite has been synthesized by two-stage process. The first stage in the process was the precipitation of Zn, Mn and Fe hydroxides from sulphate solutions, and the next was the synthesis of a precursor by the sol–gel auto-combustion method. The chemical and structural changes that occur in as-obtained material were studied. We think that the obtain results can be the basis for further research into the possibility of formation Mn–Zn ferrite from sulphate solutions after the acid leaching of battery waste. The method proposed in this study seems to be attractive because of energy-saving. It is also inexpensive and allows to synthesis nanometric and homogeneous material.

Experimental

Materials

$Mn_{0.6}Zn_{0.4}Fe_2O_4$ ferrite was produced by two-step method: co-precipitation metals sulphate into hydroxide precipitate and then synthesizing a ferrite precursor by the sol–gel auto-combustion method. The reagents were: iron(II) sulphate $FeSO_4{\cdot}7H_2O$, zinc sulphate $ZnSO_4{\cdot}7H_2O$, manganese(II) sulphate $MnSO_4{\cdot}H_2O$ and citric acid $C_6H_8O_7$, concentrated nitric(V) acid HNO_3, 2 M sulphuric(VI) acid H_2SO_4, 2 M solution of sodium hydroxide NaOH and 25% by vol. aqueous ammonia solution $NH_3{\cdot}H_2O$. All the reagents were of analytical grade.

First appropriate amount of $FeSO_4{\cdot}7H_2O$, $ZnSO_4{\cdot}7H_2O$ and $MnSO_4{\cdot}H_2O$ was dissolved in distilled water, and then 2 M H_2SO_4 was added to maintain the metal ion oxidation state of +2. Precipitation was carried out using 25% vol. of $NH_3{\cdot}H_2O$ or 2 M NaOH. An experimentally selected precipitating agent was added portionwise to the metal sulphates solution under magnetic stirring. Precipitation was conducted at a temperature of 60 °C until the solution's pH stabilized at about 10. The precipitate was filtered, washed and dried overnight at a temperature of 110 °C. These conditions were previously optimized and described [21].

The next stage in ferrite precursor synthesis was the sol–gel auto-combustion process which was conducted for two molar ratios fuel (F) to total amount of metal ions in solution (M) F:M = 1:1 and 2:1. A stoichiometric amount of citric acid was dissolved in distilled water. The previously dried hydroxide precipitate was ground in a mortar and added to the citric acid. Concentrated HNO_3 was dropwise added to this mixture and heated until the hydroxide precipitate dissolved. Subsequently, 25% vol. $NH_3{\cdot}H_2O$ was added until pH = 7 was obtained. Heating was continued until gel formed. The treatment of the obtained gel depended on the used molar ratio F:M. In the case of the sample with F:M = 2:1, the further heating of the gel (on the stirrer) would lead to auto-combustion within the reaction vessel, whereas the sample with F:M = 1:1 required greater air access to the combustion reaction, and so the predried gel was reduced to ashes in a furnace.

The powder after ashing at 420 °C was isostatic pressed in the shape of a toroid and high-temperature sintered at 1300 °C under air. The density of so prepared product was determined on the basis of Archimedes' principle.

Techniques

ICP-AES, X-ray powder diffraction, TG/DTA, FTIR spectroscopy, BET and SEM were used to investigate the synthesized ferrites.

The quantitative chemical analysis of Fe, Zn and Mn ions for filtrate and for ferrite samples dissolved in HCl was determined by ICP-AES method (Liberty, Varian).

The phase purity of the reagents and phase structure of products were controlled and identified by powder X-ray diffraction at room temperature on a Siemens D 5000 diffractometer (CuKα-radiation). Average crystallite size was estimated from XRD measurements by Scherrer equation:

$$D = 0.9\lambda/(B - B_0)\cos\theta,$$

where D is the mean crystallite size in the direction perpendicular to the (hkl) plane of reflexes in nanometre, K is a Scherrer constant, $\lambda = 0.154$ nm, B and B_0 is the

full-width at half-maximum (FWHM) of diffraction peak at angle θ and the corrected instrumental broadening in rad, respectively. In this article, the (311) peak was chosen for calculations as the most suitable for crystallite size determination. The $K = 0.9$ was used in calculations as proposed by Klug et al. [22]. The precision of the crystallites size estimation (usually 10–20%) is dependent on particles geometry and size distribution.

The DTA heating was carried out with a derivatograph type 3427 (MOM, Hungary), up to 1350 °C (heating rate: 7.5 K min^{-1}, reference material: α-alumina, platinum crucibles, Pt/PtRh10 thermocouple) under air.

A Fourier transform IR spectrometer (PERKIN-ELMER SYSTEM 2000 FTIR) was used to record IR spectra of the samples in KBr pressed pellets in the range of wavenumbers 400–4000 cm^{-1}.

The specific surface area value and pore size distributions were determined by multipoint BET method by nitrogen adsorption using Autosorb 1, Quantachrome Autosorb Automated Gas Sorption System (Quantachrome Instruments).

The microstructure of the ferrites obtained at a temperature of 420 and 1300 °C was examined by a scanning electron microscope (JOEL JSM-5800LV).

Results and discussion

The yield of metal precipitation from the sulphate solutions for the precipitants: NaOH and NH_4OH was ascertained by the inductively coupled plasma optical emission spectrophotometry (ICP-AES) technique, by determining the Fe, Zn and Mn ion content in the filtrate after precipitation. The results show that in the metal precipitation conditions defined above, the yield of precipitation with NaOH as the precipitating agent is higher. The precipitation yield of Fe, Zn and Mn amounts: 99.91, 99.95 and 98.55%, respectively. When Fe, Zn and Mn were precipitated with 25% vol. $NH_3 \cdot H_2O$, the metal hydroxides did not precipitate completely. The lower metal precipitation yield (99.1, 85.6 and 95.2% for Fe, Zn and Mn) in the case of the ammonia solution may due to the formation of soluble Zn and Mn complexes, which is mentioned by Rath et al. [10].

The applied oxidizer/metal ions molar ratio had a significant effect on the gelation process. Hence, the two products: the ferrite powder after ashing at 420 °C and the ferrite powder after auto-combustion were subjected to mineralization in HCl, and the stoichiometry of the particular ferrite components (Fe, Zn and Mn) in them was determined by ICP-AES. In both cases, the obtained material contains about 21 mol% less Zn than the assumed amount, but spinel phase occurs in a wide range of composition. The detected lower Zn content may be connected with the gel ashing and auto-combustion process conditions since the temperature resulting from the combustion considerably exceeds the zinc oxide sublimation temperature (1800 °C), and the vigorous gas evolution accelerates the loss of zinc from the material volume. The zinc loss during sintering is widely known in traditional method of synthesis ferrite materials [23]. Finally, ferrite with the composition: $Mn_{0.68}Zn_{0.32}Fe_2O_4$ is obtained.

A powder X-ray analysis of a gel sample ashed at a temperature of 420 °C for 1 h and of samples sintered in air at a temperature of 720, 1150 and 1300 °C (Fig. 1) show that a spinel phase (ICDD; PDF 10-0467) forms already during combustion, for both the powder ashed at 420 °C and the one obtained as a result of auto-combustion. The reflections characteristics of the spinel phase are not intensive (Fig. 1a), which may indicate low crystallinity and/or small particle size. Besides the spinel phase, sharp reflections characteristics of phase α-Fe_2O_3 occur in the spectrum of the sample sintered at 720 °C (Fig. 1b). The formation of a hematite phase was also confirmed by DTA/TG for ferrite powder heated to 1300 °C under air (a change in mass associated with the formation of α-Fe_2O_3 was visible in the TG curve). The formation of this intermediate phase may be caused by the excessive (relative to zinc) Fe content in the sample, due to a zinc loss of about 21 mol% during ashing and auto-combustion. This was confirmed by an ICP analysis. According to Waqas and Ping Hu et al. [5, 24], at low temperatures, the partial pressure of oxygen is higher than the ferrite decomposition pressure. The above authors prove that in such conditions

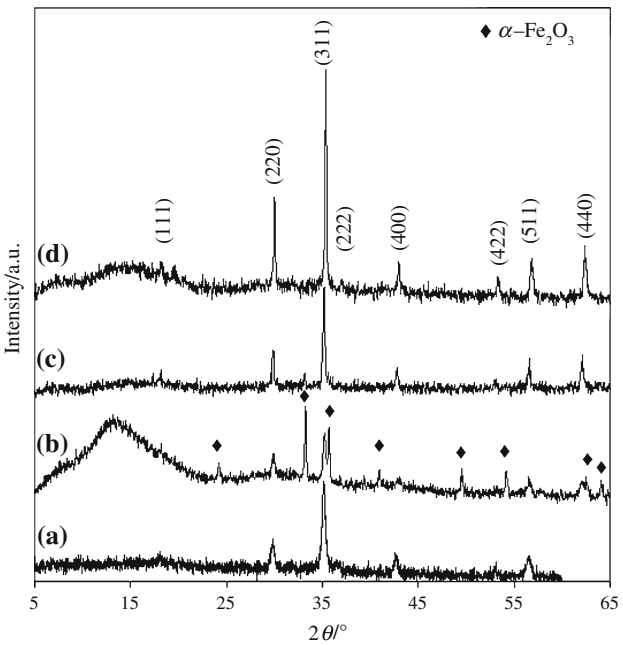

Fig. 1 XRD spectra for powder after annealing at **a** 420 °C, **b** 720 °C, **c** 1150 °C and **d** 1300 °C

some of the ferrite undergoes oxidation with forming intermediate phases: Mn_2O_3 and α-Fe_2O_3 with a body-centred cubic structure (BCC) which does not solve in the spinel structure. It could have been explained either amorphous/non-crystalline nature of this phase or its content is too low to detect by XRD analysis. At a higher temperature, the phases again build into the spinel structure [24]. Consequently, for the samples sintered at higher temperatures (1150 and 1300 °C), no peaks characteristics of α-Fe_2O_3 (ICDD; PDF 33-0664) appear in the XRD spectra (Fig. 1c, d), whereas the reflections characteristics of the spinel phase are intensive and sharp, which is associated with increased crystallinity of the Mn–Zn ferrite at higher temperatures.

The particle size of the ferrite powder after ashing, calculated from the Scherrer equation for the peak (311) at $2\theta = 34.99^{\circ}$, is 28.1 nm, whilst for the ferrite obtained from auto-combustion it amounts to 66.6 nm.

The gel ashing temperature and time optimum for the formation of a ferrite precursor were determined by DTA/TG. Figure 2a–c shows heating T/TG/DTA curves of the samples ashed at 420 °C for 15, 30 and 60 min, respectively. The significant (about 90%) mass loss was observed on TG curve at 350 °C for sample ashed for 15 min (Fig. 2a) and two strong exothermic effects (corresponded to this mass loss) associated with the combustion of the gel's organic components are reflected in the DTA curve in the temperature range of 300–500 °C. When the ashing time was extended to 30 min (Fig. 2b), a small wide peak occurs on the DTA curve at a temperature of about 300 °C and the corresponding mass decrement on the TG curve is small (10%). For an ashing time of 1 h, no changes on the TG curve were denoted in a temperature range of 300–700 °C (Fig. 2c). Whereas for the samples ashed for respectively 30 min and for 1 h, slight (about 8 wt%) mass decrements occur on the TG curve at a temperature of about 700 °C. They are probably connected with the formation of phase α-Fe_2O_3, as confirmed by XRD results (Fig. 1b).

The chemical and structural changes taking place in the material during auto-combustion can be determined using spectroscopic techniques. Figure 3 shows FTIR spectra for samples of gel and powder (obtained in the SC process from the precursor precipitated with NaOH) after auto-combustion, whilst spectra for the powder produced by combusting gel obtained in the SC process from the precursor precipitated with the ammonia solution are shown in Fig. 4. In the case of each of the ferrite powder samples after combustion, a band characteristic of water particle stretching and deformation vibrations (3400 and 1630 cm^{-1}) occurs. For gel (Fig. 3a) in the range of 1384 and 830 cm^{-1}, there are bands originating from the asymmetric stretching vibrations of the remaining NO_3^- particles (the SC process oxidizer) and bond C=O at 1550 cm^{-1} (originating from the citric acid), which in the spectrum (Fig. 3b) of the post-combustion sample is less intensive [25].

At 1120 cm^{-1} and 980 cm^{-1} in the IR spectrum of the samples obtained in the SC process from the precursor precipitated with the ammonia solution (Fig. 4), there are bands characteristic for respectively group SO_4^{2-} and group NH_4^+. It appears from the above that $(NH_4)_2SO_4$ particles are occluded during metal precipitation with ammonia [26].

The IR spectrum for the sample obtained from auto-combustion and the sample ashed at 420 °C shows radiation absorption ca of about 550 cm^{-1}, characteristic of interactions between oxygen and the metal cation occupy octa or tetrahedral sites in the spinel structure [8]. Hence one can conclude that Mn–Zn ferrite forms after both ashing and auto-combustion. However, the kind of the precipitating agent used to obtain the hydroxide precipitate subsequently used in the SC process has a significant effect on the purity of the obtained material. NaOH not only makes precipitation more efficient, but also prevents contaminations.

Figure 5 presents the recorded nitrogen adsorption–desorption isotherms of Mn–Zn ferrite powder prepared by ashing at a temperature of 420 °C and calcined at 720 °C. Both adsorption isotherms are convex in the whole pressure range and can be considered as a combination of the Type III and V as a result of the presence of various kinds of pores in structure, mainly of macropores (>50 nm) with a slight mesopores (below 2–50 nm in diameter) fraction. At relative pressures $p/p_o > 0.4$, the sample obtained at

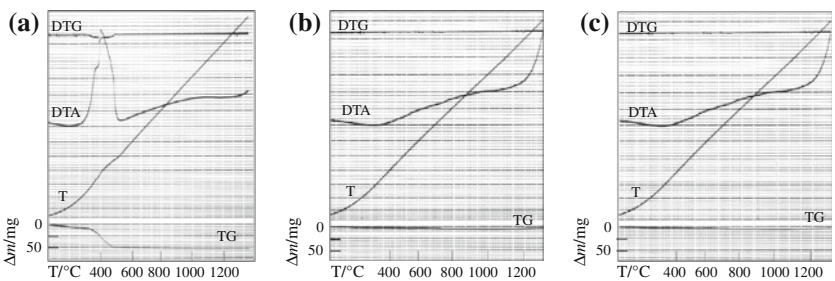

Fig. 2 The T/TG/DTA curves of the samples ashed at 420 °C for: **a** 15 min, $m = 50$ mg, **b** 30 min, $m = 30$ mg and **c** 60 min, $m = 50$ mg

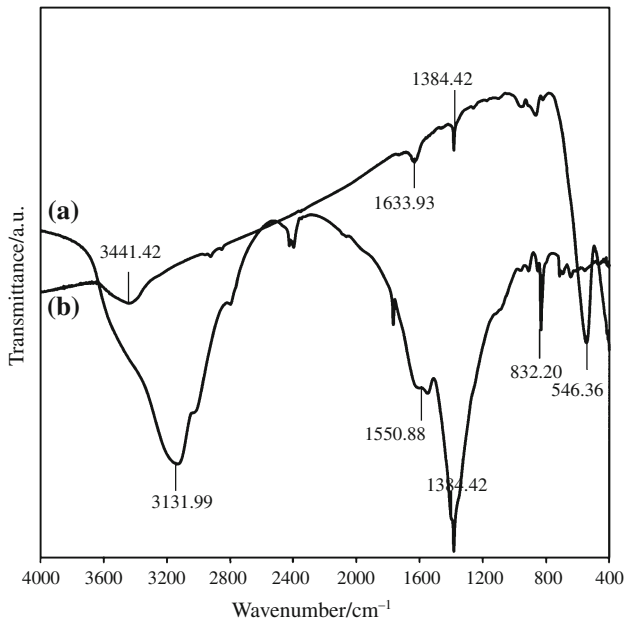

Fig. 3 IR spectrum for samples obtained after precipitation with NaOH and SC process: **a** gel and **b** powder after auto-combustion

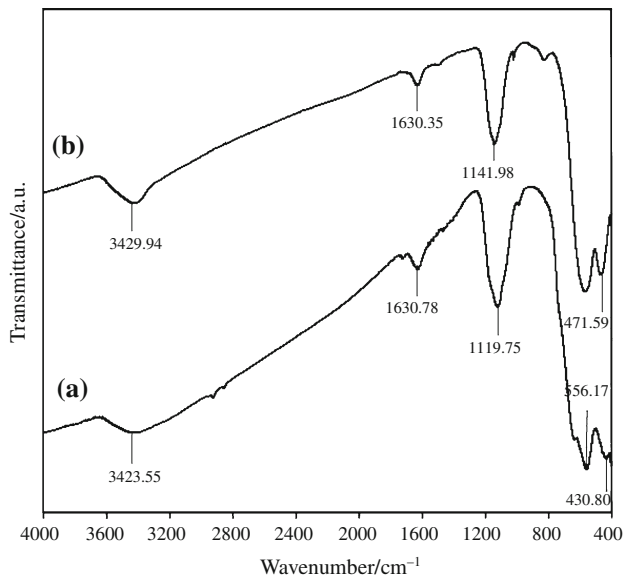

Fig. 4 IR spectrum for samples obtained after precipitation with NH_4OH and SC process: **a** powder sintered at 420 °C and **b** powder sintered at 720 °C

420 °C shows hysteresis loop seemed to be intermediate between Types H3 and H4 (Fig. 5). Type H4 loops were reported for particles with internal voids of irregular shape and broad size distribution, and it is typical of the mesoporous solids adsorption proceeding via multilayer adsorption followed by capillary condensation and isotherms with Type H3 loops were reported for solids comprised of aggregates [27]. In case of the powder sintered at

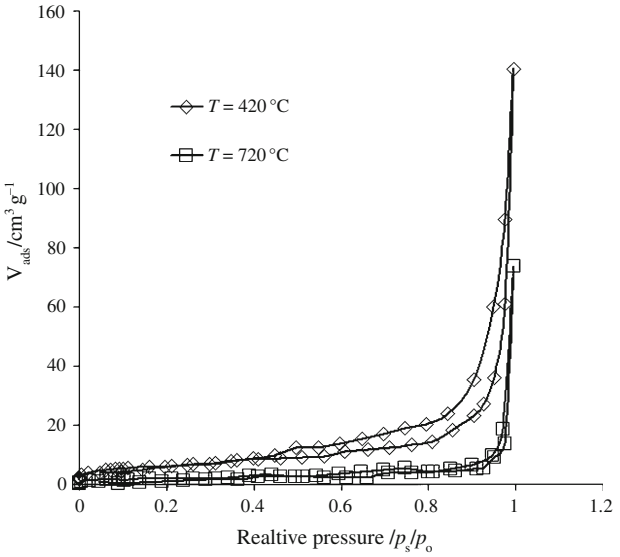

Fig. 5 N_2 adsorption (77 K) isotherms for ferrite powder produced by ashing at different temperatures

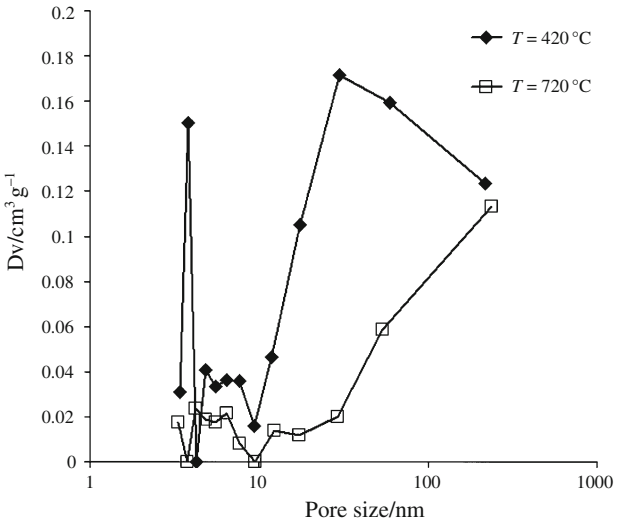

Fig. 6 Pore size distribution in ferrite powder produced by ashing at different temperatures

720 °C, the adsorption and desorption branches of the isotherm almost coincide; there is no noticeable adsorption–desorption hysteresis loop (Fig. 5).

The above interpretation is confirmed by pore size distribution diagrams (Fig. 6) where one can see that the two samples have no uniform pore structure and include mesopores and macropores. The total pore volume for the powder after ashing at 420 °C is 2.1 cm^3 g^{-1}, and it decreases almost twofold for the powder sintered of 720 °C (1.1 cm^3 g^{-1}).

The specific surface area value (determined by BET) of the ferrite powder obtained by gel ashing at 420 °C is 22.5 m^2 g^{-1}, which corresponds to small specific surface

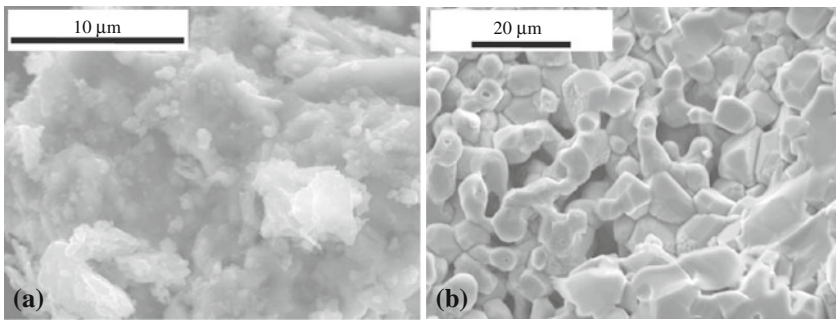

Fig. 7 SEM microphotograph for ferrite obtained at temperature: **a** 420 °C and **b** 1300 °C

development and suggests low powder crystallinity or a large amorphous phase fraction and agglomeration of particles (Figs. 1, 7). The specific surface area value markedly decreases with increasing the treatment temperature and for a sample sintered at 720 °C it amounts to 5.73 m^2 g^{-1}. The reduction in the specific surface of the powder at this temperature (720 °C) may be due to the formation of large particles of well-crystallized hematite which was shown to be present by XRD (Fig. 1b) and was confirmed by Rath et al. [10].

Figure 7 shows the SEM microphotographs of powder ashed at 420 °C and ferrite powder in the shape of a toroid obtained through isostatic pressing and high-temperature sintering at 1300 °C under air. In the image of the ashed sample (Fig. 7a), not very dense agglomeration (1–5 μm) of fine particles is visible that may be due to interactions between magnetic nanoparticles. It seems that spherical particles predominate, but because of the agglomeration it is difficult to estimate the average particle size from SEM. In the second case, in which the powder was subjected to conventional sintering (Fig. 7b), the well-densified and homogenous microstructure can be observed. The particle size distribution is uniform, and the average grain size is ca 5 μm, that is smaller than in conventional method (grain size in conventional route is > 10 μm). As could be expected, the average particle size increases with treatment temperature; the particle size formed from the gel by ashing was much smaller than that obtained during calcination at 1300 °C. The results of the microscopic analyses and their interpretation are corroborated by XRD results (Fig. 1a, d). The synthesized ferrite powder exhibited high sinterability; the density of the Mn–Zn ferrite sintered at 1300 °C, determined on the based of Archimedes' principle is 4.84 g cm^{-3} which indicates that the agglomerate is not hard and the ferrite powder was well pressed and sintered.

This research results indicates that there is a possibility to synthesize of nanocrystalline Mn–Zn ferrite by proposed two-stage route: the precipitation of Zn, Mn and Fe hydroxides from sulphates solution and the synthesis of a precursor by the sol–gel auto-combustion method. The solution after the acid leaching of battery waste can be utilized as a starting material in Mn–Zn ferrite synthesis.

Conclusions

Nanocrystalline Mn–Zn ferrite was produced from solutions of Zn, Mn and Fe sulphates by the sol–gel auto-combustion method. The X-ray powder diffraction shows that a spinel phase forms already after this material treatment stage. The particle size of the powders, calculated by the Scherrer method, amounts to 28.1 nm for the sample ashed at 400 °C and 66.6 nm for the sample after auto-combustion. The powder ashed at a lower temperature has a relatively small specific surface area (22.5 m^2 g^{-1}). As the gel is being ashed in auto-combustion conditions, a considerable amount of zinc is lost from the material volume, which may be due to the exceeding of the ZnO sublimation temperature. The sintering of the powder under air at a higher temperature favours the formation of phase α-Fe_2O_3, which above 1000 °C again dissolves in the spinel phase. A pure spinel phase was obtained when the ferrite powder was pressed and sintered at 1300 °C, and the material had a well-densified homogenous microstructure with average grain size smaller compared with ferrites prepared by the conventional method.

From the investigation, we can conclude that the sol–gel auto-combustion method can be applied to the solution after the acid leaching of battery waste containing Fe, Zn and Mn sulphates to obtain nanocrystalline Mn–Zn ferrite.

References

1. Dasguptaa S, Dasb J, Eckertb J, Mannaa I. Influence of environment and grain size on magnetic properties of nanocrystalline Mn–Zn ferrite. J Magn Magn Mater. 2006;306:9–15.
2. Goldman A. Modern ferrite technology. 2nd ed. Pittsburgh: Springer; 2006.
3. Schaller GE. Ferrite processing & effects on material performance, Ceramic Magnetics. http://www.cmi-ferrite.com/.

4. Waqas H, Qureshi AH. Influence of pH on nanosized Mn–Zn ferrite synthesized by sol–gel auto combustion process. J Therm Anal Calorim. 2009;98:355–60.
5. Waqas H, Qureshi AH. Low temperature sintering study of nanosized Mn–Zn ferrites synthesized by sol–gel auto combustion process. J Therm Anal Calorim. 2010;100:529–35.
6. Thakur A, Singh M. Preparation and characterization of nanosize $Mn_{0.4}Zn_{0.6}$ Fe_2O_4 ferrite by citrate precursor method. Ceram Int. 2003;29:505–11.
7. Azadmanjiri J. Preparation of Mn–Zn ferrite nanoparticles from chemical sol–gel combustion method and the magnetic properties after sintering. J Non-Cryst Solids. 2007;353:4170–3.
8. Yan S, Ling W, Zhou E. Rapid synthesis of $Mn_{0.65}Zn_{0.35}Fe_2O_4$/$SiO_2$ homogeneous nanocomposites by modified sol–gel autocombustion method. J Cryst Growth. 2004;273:226–33.
9. Mangalaraja RV, Ananthakmar S, Manohar P, Gnanam FD, Awano M. Characterization of $Mn_{0.8}Zn_{0.2}Fe_2O_4$ synthesized by flash combustion technique. Mater Sci Eng A. 2004;367:301–5.
10. Rath C, Sahu KK, Anand S, Date SK, Mishra NC, Das RP. Preparation and characterization of nanosize Mn–Zn ferrite. J Magn Magn Mater. 1999;202:77–84.
11. Wang J, Zeng C, Peng Z, Chen Q. Synthesis and magnetic properties of $Zn_{1-x}Mn_xFe_2O_4$ nanoparticles. Physica B. 2004;349:124–8.
12. Arulmurugana R, Vaidyanathan G, Sendhilnathan S, Jeyadevan B. Mn–Zn ferrite nanoparticles for ferrofluid preparation: study on thermal–magnetic properties. J Magn Magn Mater. 2006;298:83–94.
13. Mathew DS, Juang R-S. An overview of the structure and magnetism of spinel ferrite nanoparticles and their synthesis in microemulsions. Chem Eng J. 2007;129:51–65.
14. Giri J, Srihasha T, Asthana S, Gundu Rao TK, Nigam AK, Bahadur D. Synthesis of capped nanosized $Mn_{1-x}Zn_xFe_2O_4$ ($0 \leq x \leq 0.8$) by microwave refluxing for bio-medical applications. J Magn Magn Mater. 2005;293:55–61.
15. Pradhan P, Giri J, Banerjee R, Bellare J, Bahadur D. Preparation and characterization of manganese ferrite-based magnetic liposomes for hyperthermia treatment of cancer. J Magn Magn Mater. 2007;311:208–15.
16. Ito A, Shinkai M, Honda H, Kobayashi T. Medical application of functionalized magnetic nanoparticles. J Biosci Bioeng. 2005;100:1–11.
17. Kadu AV, Jagtap SV, Chaudhari GN. Studies on the preparation and ethanol gas sensing properties of spinel $Zn_{0.6}Mn_{0.4}Fe_2O_4$ nanomaterials. Curr Appl Phys. 2009;9:1246–51.
18. Klimkiewicz R, Przybylski K, Baran J, Mińta W. Mg−Zn and Mn−Zn ferrites derived from coil core materials as new precursors for catalysts of primary alcohols transformations. Ind Eng Chem Res. 2009;48:6291–5.
19. Patil KC, Aruna ST, Ekambaram S. Combustion synthesis. Curr Opin Solid State Mater Sci. 1997;2:158–65.
20. Mukasyan AS, Epstein P, Dinka P. Solution combustion synthesis of nanomaterials. Proc Combust Inst. 2007;3:1789–95.
21. Winiarska K, Zabłocka-Malicka M. Prace Naukowe Wydziału Chemicznego Politechniki Wrocławskiej nr 6, Wrocław; 2006 (in Polish).
22. Klug HP, Alexander LE. X-ray diffraction procedures for polycrystalline and amorphous materials. New York: Willey & Sons; 1974.
23. Chen SH, Chang SC, Lin IN, Tung MJ, Shu WB. Effect of sintering parameters on Zn loss for preparation of high permeability MnZn ferrites. IEEE Trans Magn. 1992;28:2436–8.
24. Hu P, Yang H, Pan D, Wang H, Tian J, Zhang S, Wang X, Volynsky AA. Heat treatment effects on microstructure and magnetic properties of Mn–Zn ferrite powders. J Magn Magn Mater. 2010;322:173–7.
25. Pouchert C. The Aldrich library of FT-IR spectra. 2nd ed. Milwaukee: Aldrich; 1997.
26. López FA, López-Delgado A, Martín de Vidales JL, Vila E. Synthesis of nanocrystalline zinc ferrite powders from sulphuric pickling waste water. J Alloy Compd. 1998;265:291–6.
27. Kruk M, Jaroniec M. Gas adsorption characterization of ordered organic−inorganic nanocomposite materials. Chem Mater. 2001;13:3169–83.